IEEE Photonics Journal
An IEEE Photonics Society Publication

Open Access

Optical Cavity Effects in InGaN Micro-Light-Emitting Diodes With Metallic Coating

Volume 9, Number 3, June 2017

Hong Chen
Houqiang Fu
Xuanqi Huang
Zhijian Lu
Xiaodong Zhang
Jossue Montes
Yuji Zhao

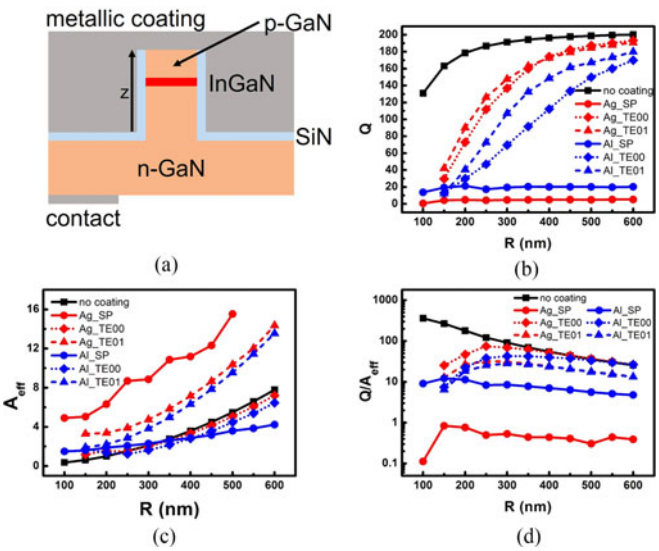

DOI: 10.1109/JPHOT.2017.2690389
1943-0655 © 2017 IEEE

IEEE photonics SOCIETY

IEEE

Optical Cavity Effects in InGaN Micro-Light-Emitting Diodes With Metallic Coating

Hong Chen, Houqiang Fu, Xuanqi Huang, Zhijian Lu, Xiaodong Zhang, Jossue Montes, and Yuji Zhao

School of Electrical, Computer, and Energy Engineering, Arizona State University, Tempe, AZ 85287 USA

DOI:10.1109/JPHOT.2017.2690389

Manuscript received March 1, 2017; revised March 24, 2017; accepted March 28, 2017. Date of publication April 12, 2017; date of current version April 19, 2017. This work was supported by the Bisgrove Scholar Program from Science Foundation Arizona. Corresponding author: H. Chen (e-mail: hchen170@asu.edu).

Abstract: We implement finite difference method (FDM) to calculate the optical cavity effects in InGaN micro-light-emitting diodes (LEDs) with metallic coating. The dispersion relation, mode profile, energy density W of electromagnetic field, cavity quality factor Q, and effective mode area A_{eff} are theoretically investigated. The results show that although the strongest confinement of the field is achieved by surface plasmon modes at GaN/Ag interface, the energy density W is small inside the cavity, leading to a high effective mode area. Additionally, the cavity without metallic coating has the highest Q factors since no metal loss is involved. These results can serve as guidelines for the design and fabrication of high efficiency and high speed LEDs for the applications of solid-state lighting and visible-light communication.

Index Terms: Light-emitting diodes (LEDs), plasmonics, waveguides.

1. Introduction

III-nitride materials have enabled a variety of applications including solid-state lighting [1]–[3] full-color displays [4], solar cells [5], and intersubband transition optoelectronic devices [6]. Recently, visible light communication (VLC) in free space using micro-light-emitting diodes (mLED) based on III-nitride material has attracted tremendous attentions [7]–[11] due to its large modulation bandwidth, easy integration, and high energy efficiency. In order to increase the modulation speed of mLED, high spontaneous recombination rates are desirable. The recombination rates of traditional light-emitting diodes (LEDs) based on InGaN quantum wells (QWs), however, are restricted by the quantum confined Stark-effect (QCSE) owing to the strong internal polarization-related fields on the c-plane [12]. In order to address these issues, novel nonpolar and semipolar InGaN LEDs have been implemented and have demonstrated higher recombination rates [13]–[16]. Recently, to further increase the spontaneous recombination rate, surface plasmon (SP) enhanced spontaneous emission inside QWs has been proposed and has shown significant improvement on the modulation response [8], [17]–[19]. Our previous work studied the enhancement of the spontaneous recombination rates of semipolar GaN LEDs coated with metallic gratings [8], and the result showed that 3-dB modulation frequency of 5.4 GHz could be obtained. In addition to metallic thin film or metallic

grating coated InGaN QW LEDs, another approach involves utilizing the nano LED structures with metallic coating [3], [20]–[23]. Recent theoretical works [20], [21] on the core-shell nano LED structures show that the modulation speed of LEDs could be increased by metallic coatings. However, the impact from metallic coating for mLED structures have not been fully investigated yet. In this work, we theoretically study the optical cavity effects in mLEDs with metallic coating using the finite difference method (FDM) where TE-like and SP modes are investigated. Unlike nano LEDs grown by MOCVD or MBE [3], the micro InGaN LEDs structure studied in this work can be fabricated by depositing metals onto mLEDs etched by reactive ion etching process. Previous theoretical studies are based on the finite difference time domain (FDTD) method [20], [21], which provides information on Purcell factor and light extraction efficiencies. In this work, in order to understand the optical properties of different modes, FDM is implemented, optical properties such as dispersion relation, mode profile, energy density of the electric field, quality factor and effective mode volume are investigated. In order to study correlation between the surface plasmon resonance frequency and the QW emission frequency, we choose silver and aluminum as two different coating materials, referring to the case of emission frequency near resonance frequency and emission frequency far away from resonance frequency, respectively [17]. The work is organized as follows: In Section 2, we describe the theoretical background and simulation methods; in Section 3-1, dispersion relation of different types of cavity modes are calculated; in Section 3-2, we compare the electric field and energy density of different modes; in Section 3-3, quality factor and effective mode volume are studied. The results of this work can be used to guide the design of micro InGaN LEDs for the applications of solid-state lighting and visible-light communication.

2. Simulation Method

2.1 Theoretical Background

In this work, the wave vector and the electromagnetic field are calculated by the FDM method. The quality factor Q is calculated by (1), where k_{real} and k_{imag} indicate the real and imaginary part of the wave vector, respectively. For the total Q factor in a real cavity, $1/Q_{\text{total}} = 1/Q_{\text{rad}} + 1/Q_{\text{cavity}}$, where Q_{rad} accounts for the radiation loss and Q_{cavity} accounts for the loss inside cavity. The Q calculated in this work only considers Q_{cavity}; when the device is a laser, there is reflection and/or scattering happening at the terminus of the cavity that is also related to the coating materials. This issue exceeds the scope of this research but is valuable to study [24]. For the mode volume, we choose the definition of effective mode area [25], [26] to describe the confinement in the lateral dimension (perpendicular to the growth direction) given by (2), where A_{eff} represents the effective mode area, W represents the energy density of electromagnetic field, and $W(x_0, y_0)$ represents the energy density at the location where the emitter exists. For the confinement along the vertical direction (parallel to the growth direction), since the device studied in this work is an LED, we assume the mode volume is the same due to the same cavity geometry:

$$Q = k_{\text{real}}/2k_{\text{imag}} \tag{1}$$

$$A_{eff} W(x_0, y_0) = \int W(x, y) dx dy. \tag{2}$$

For the energy density of the electromagnetic filed, noting that traditional definitions could lead to an imaginary or negative energy density, we choose the equation developed in [27], given by (3), the ϵ_0 indicates electric constant of free space, n, k the real and imaginary part of refractive index, respectively, ω the angular frequency of light, Γ_e the damping frequency. Parameters in (3) can be found from [28] for silver and aluminum:

$$W = \frac{\epsilon_0}{2}(n^2 + 2\omega nk/\Gamma_e)\,|E|^2\,. \tag{3}$$

For TE-like modes inside cavity, we choose the maximum energy density location in the semiconductor region, while for the SP modes, since the maximum energy density is achieved at the surface, we place the emitter 10 nm away from the metal interface.

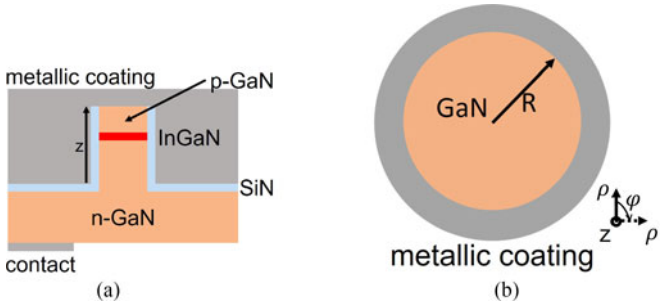

Fig. 1. (a) Micro LED structure. (b) Structure simulated in this study.

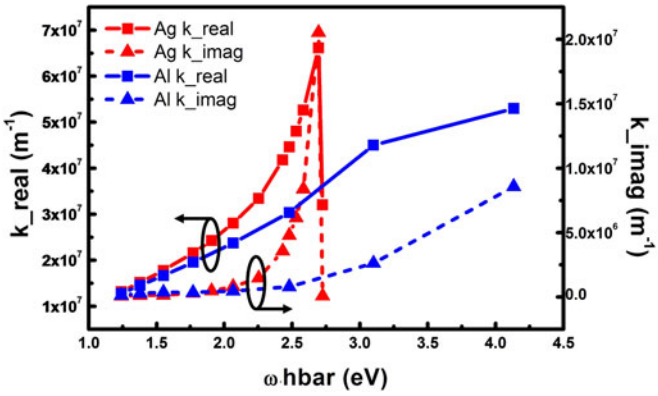

Fig. 2. Dispersion relation of surface plasmon mode at GaN/metal interface. The metals are silver and aluminum in this study. The radius of core region is 500 nm.

2.2 Set-up of the Simulation

A commercial FDM package (Lumerical Mode solutions) is used in this work. We simplify this study to a 2-D waveguide problem by calculating modes in cross section shown in Fig. 1(b). Note that the silicon nitride and the InGaN layers are usually on the order of nanometers [17], [29], [30], which is thin enough compared to the diameter and the vertical length of the cavity coated by the metal, respectively. Therefore, both layers are omitted in Fig. 1(b) for simplicity. The influence from dielectric layer is studied in [31] in $In_{0.53}$ $Ga_{0.47}$ As nano cavity, the refractive index of $In_{0.53}$ $Ga_{0.47}$ As is larger than 3.5, for silicon nitride $n = 1.99$ at 1550 nm, while in this work, the refractive index of GaN ($n = 2.4$) and silicon nitride ($n = 2.04$) are comparable; thus, the dielectric layer should not give significant influence in this work. Thickness of the coated metallic layer is assumed to be infinite since the wave decays quickly inside the metallic layer. Solving the modes at cross-section inside the cavity by FDM, the effective mode area A_{eff}, and wave vectors k_{real}, k_{imag} can be calculated for different core radii. The emission wavelength in this calculation is chosen to be 500 nm, and the radius of cavity varies from 100 nm to 800 nm following the typical dimensions of nanorod LEDs [32]. Dielectric functions of GaN can be found in [33].

3. Results and Discussion

3.1 Dispersion Relation of Cavity Modes

In this section, dispersion relations of the cavity modes are investigated. For SPs, the dispersion is shown in Fig. 2. The real part and imaginary part of wave vector along z direction in Fig. 1(b) is defined as k_{real} and k_{imag}, respectively.

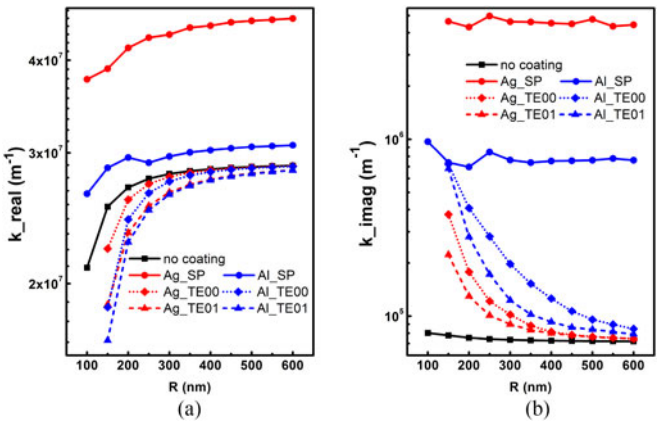

Fig. 3. (a) Real part of wave vector versus the core radius. (b) Same plot for the imaginary part of wave vector. First two orders of the TE-like modes are shown in both plots.

For SPs at GaN/Ag interface, the resonance feature is similar to previous theoretical and experimental works on planar interfaces [18], and the resonance frequency corresponds to photon energy of 2.6 eV. For GaN/Al interface the resonance frequency corresponds to 5 eV photon energy, which is away from the wavelength we studied in this work. Near the resonance frequency, huge changes of k_{real} and k_{imag} are observed, indicating an improved confinement together with an increased propagation loss. For the SP at GaN/Al interface, since large k_{real} and k_{imag} are achieved at higher frequencies in the UV region [18], therefore, at 500 nm the SPs at GaN/Al interface have relative weaker confinement and lower loss comparing with SPs at GaN/Ag interface.

In addition, the relation between wave vector and core radius are also studied, as shown in Fig. 3. It can be observed from Fig. 3(a) that k_{real} decreases with decreasing core radius. Furthermore, the k_{real} of the SP mode at the GaN/Ag interface is higher than in other modes, which is due to the surface plasmon resonance (SPR) at the emission wavelength of 500 nm. The decrease of k_{real} of SP modes is not as drastic as the decrease of TE-like modes, owing to its surface confined mode distribution property which is less sensitive to the cavity geometry. The relation between k_{imag} and core radius is shown in Fig. 3(b). High k_{imag} is observed for the SP modes. For the TE-like modes inside the cavity with metallic coating, k_{imag} increases when reducing the core radius due to the metal loss. Moreover, for the SP modes, the k_{imag} of plasmon at GaN/Ag interface is larger than that at GaN/Al interface, because the SP resonance frequency at GaN/Ag interface is near 500 nm while at GaN/Al interface the SPR frequency locates at UV region. For the TE-like modes, plasmon at GaN/Ag interface has a smaller k_{imag} compared with that at the GaN/Al interface, due to the larger extinction coefficient of the aluminum, which is an intrinsic material property [28]. For the cavity without metallic coating, the k_{imag} is small since metal loss is not involved. Noting that the cavity size is above the subwavelength level in this work, the cavity without metallic coating has the lowest loss. When the radius of cavity approaches 100 nm, TE-like modes cut off quickly but SP modes maintain constant k_{imag}, this feature agrees with studies on subwavelength region [29], [34].

3.2 Electric Field Intensity and Energy Density

The normalized electric field ($|E|^2$) and electromagnetic energy density (W) are calculated and shown in Figs. 4 and 5 for the core radius of 600 nm and 200 nm, respectively. The real and imaginary parts of the refractive index are also given. For the TE-like modes at the core radius of 600 nm, the electric field profile is similar to that of the cavity without metallic coating. For the energy density, when the electric field is not strongly confined inside the cavity, there will be a large energy

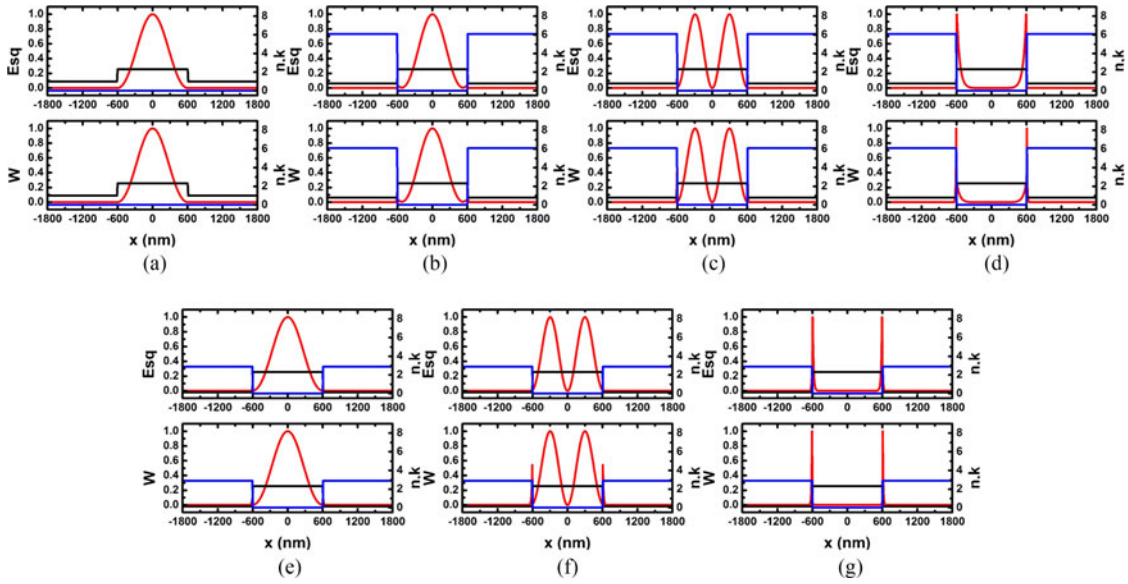

Fig. 4. Electric field squared $|E|^2$ (red line), energy density W (red line), real part of refractive index n (black line), and imaginary part of refractive index k (blue line) for (a) first order TE-like mode in cavity without coating. (b), (c) First and second order TE-like mode in cavity with aluminum coating, respectively. (d) First order SP mode in cavity with aluminum coating. (e), (f) First and second order TE-like mode in cavity with silver coating, respectively. (g) First order SP mode in cavity with silver coating. The core radius is 600 nm in this calculation.

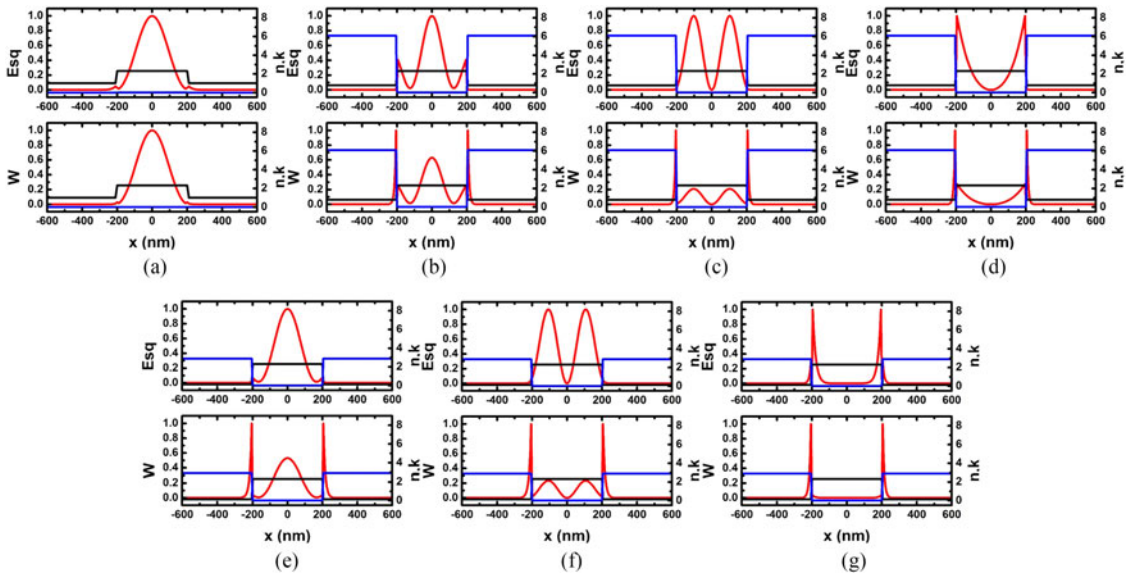

Fig. 5. Same plot as Fig. 4. The core radius is 200 nm in this calculation.

density outside the semiconductor region, owing to the large extinction coefficient k of the metal. For the SP mode, the electric field is confined at the surface as we expected, and the confinement of $|E|^2$ at the GaN/Ag interface is stronger compared with that at the GaN/Al interface, which is on account of SPR at the emission wavelength of 500 nm.

For cavity modes at the core radius of 200 nm, TE-like modes start to show hybrid properties, leading to a large energy density W outside of the cavity, while for the cavity without metallic coating, the maximum energy density W is still achieved inside the cavity.

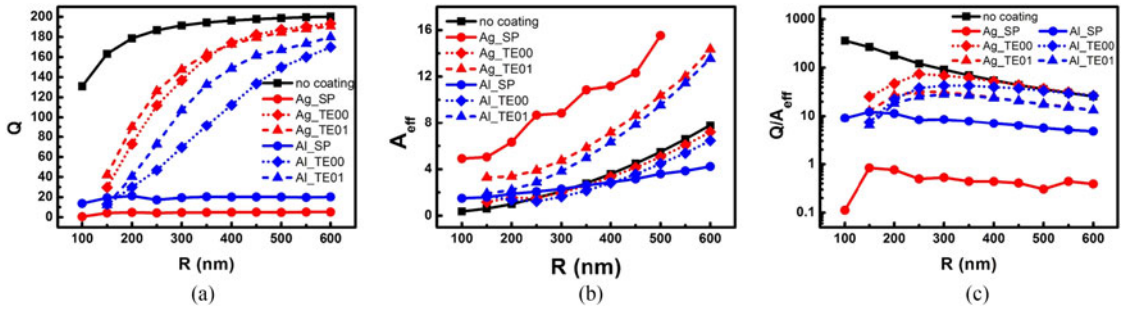

Fig. 6. (a) The Q factor of different cavity modes at different core radius, (b) effective mode area A_{eff}, (c) the ratio between Q and effective mode area.

3.3 Spectral and Spatial Energy Density

Combining the results above, the quality factor (Q) and effective mode area (A_{eff}) are calculated by utilizing (1) and (2), which describe the spectral and spatial energy density, respectively. The Q factor versus core radius is shown in Fig. 6(a). For the SP modes, it can be expected that the Q is smaller than TE-like modes due to the large imaginary part of the wave vector. Since the emission wavelength coincides with SPR at GaN/Ag interface, the SP modes of the silver-coated cavity give the smallest quality factor. It can also be observed that the TE-like mode inside the cavity without a metallic grating has the highest Q factor due to the smallest k_{imag}. The effective mode area is given by Fig. 6(b). Even though the SP mode at the GaN/Ag interface has the strongest confinement, since the emitters can only exist inside the cavity (10 nm away from the metal inside the cavity in this calculation), the coupling strength from the emitter to the SP mode is small, which increases the effective mode area of the SP modes. The ratio between Q factor and the effective mode area is given in Fig. 6(c). Since the device in this study is an LED, the vertical length can be assumed to be sufficiently large and thus the same for each mode. Thus, the value of Q/A_{eff} can also provide the information of Q/V_{eff} since the vertical length can be removed from the reduction of a fraction, which is related to, e.g., the enhanced spontaneous emission inside the cavity.

When the size of the cavity is reduced, both Q and A_{eff} of TE-like modes are reduced. For the plasmonic mode, the Q factor is insensitive to the size, but A_{eff} is reduced. From Fig. 6(c), it can be observed that the cavity without metallic coatings gives the highest enhancement to the optical transitions inside the cavity. Noting that the vertical dimension is assumed to be sufficiently large, the wave vector along the propagation direction does not influence the effective mode volume. For devices where vertical confinement is important (such as lasers [35], [36]), the reflection and scattering happening at the terminus of the cavity is strongly related to the coating material, thus the total Q factor could be different from the result in this work. On the other hand, the large wave vector of SP modes could further reduce the mode volume, leading to different conclusions from this work. For cavities above subwavelength region, surface plasmon enhanced spontaneous emission may not be feasible due to the high loss and the large distance from emitter to the interface. Cavities without metallic coatings gives the highest Q/V_{eff}.

In a short conclusion, cavity without metallic coating gives the lowest loss and strongest effective mode area when the cavity size is reduced, which can be attributed to the small imaginary part of the wave vector, large Q/A_{eff} has the potential to enhance the spontaneous emission rate. Metal loss makes the Q/A_{eff} of TE-like modes inside cavity lower comparing with cavity without coating. For SPs, Ag coated cavity has lowest Q/A_{eff} due to large imaginary part of wave vector near resonance frequency, while Al coated cavity has relative higher Q/A_{eff} since the wavelength is far away from the resonance frequency at Al/GaN interface.

4. Conclusion

This work studied the cavity effects in mLEDs with metallic coating. Different types of modes were investigated. The SP mode at GaN/Ag interface has the lowest quality factor and the highest effective mode area, leading to the lowest Q/A_{eff}, the counterintuitive observation is due to the small energy density inside the cavity. Higher Q/A_{eff} are achieved by TE-like mode. The cavity without metallic coating has the highest Q factor and highest Q/A_{eff} since no metal loss is involved. Such a high Q/A_{eff} has the potential to enhance spontaneous emission rates.

References

[1] M. Krames *et al.*, "High-power III-nitride emitters for solid-state lighting," *Physica Status Solidi a*, vol. 192, no. 2, pp. 237–245, 2002.
[2] D. F. Feezell, J. S. Speck, S. P. DenBaars, and S. Nakamura, "Semipolar InGaN/GaN light-emitting diodes for high-efficiency solid-state lighting," *J. Display Technol.*, vol. 9, no. 4, pp. 190–198, 2013.
[3] S. Li and A. Waag, "GaN based nanorods for solid state lighting," *J. Appl. Phys.*, vol. 111, no. 7, 2012, Art. no. 071101.
[4] F. Qian, S. Gradecak, Y. Li, C.-Y. Wen, and C. M. Lieber, "Core/multishell nanowire heterostructures as multicolor, high-efficiency light-emitting diodes," *Nano Lett.*, vol. 5, no. 11, pp. 2287–2291, 2005.
[5] X. Huang, H. Fu, H. Chen, Z. Lu, D. Ding, and Y. Zhao, "Analysis of loss mechanisms in InGaN solar cells using a semi-analytical model," *J. Appl. Phys.*, vol. 119, no. 21, 2016, Art. no. 213101.
[6] H. Fu, Z. Lu, X. Huang, H. Chen, and Y. Zhao, "Crystal orientation dependent intersubband transition in semipolar AlGaN/GaN single quantum well for optoelectronic applications," *J. Appl. Phys.*, vol. 119, no. 17, 2016, Art. no. 174502.
[7] J. J. McKendry *et al.*, "High-speed visible light communications using individual pixels in a micro light-emitting diode array," *IEEE Photon. Technol. Lett.*, vol. 22, no. 18, pp. 1346–1348, Sep. 2010.
[8] H. Chen, H. Fu, Z. Lu, X. Huang, and Y. Zhao, "Optical properties of highly polarized InGaN light-emitting diodes modified by plasmonic metallic grating," *Opt. Exp.*, vol. 24, no. 10, pp. A856–A867, 2016.
[9] J. J. McKendry *et al.*, "Visible-light communications using a CMOS-controlled micro-light-emitting-diode array," *J. Lightw. Technol.*, vol. 30, no. 1, pp. 61–67, 2012.
[10] C. Du *et al.*, "Tuning carrier lifetime in InGaN/GaN LEDs via strain compensation for high-speed visible light communication," *Sci. Rep.*, vol. 6, 2016, Art. no. 37132.
[11] R. X. Ferreira *et al.*, "High bandwidth GaN-based micro-LEDs for multi-Gb/s visible light communications," *IEEE Photon. Technol. Lett.*, vol. 28, no. 19, pp. 2023–2026, Oct. 2016.
[12] P. Waltereit *et al.*, "Nitride semiconductors free of electrostatic fields for efficient white light-emitting diodes," *Nature*, vol. 406, no. 6798, pp. 865–868, 2000.
[13] Y. Zhao *et al.*, "High-power blue-violet semipolar (2021) InGaN/GaN light-emitting diodes with low efficiency droop at 200 A/cm^2," *Appl. Phys. Exp.*, vol. 4, no. 8, 2011, Art. no. 082104.
[14] Y. Zhao *et al.*, "Green semipolar (2021) InGaN light-emitting diodes with small wavelength shift and narrow spectral linewidth," *Appl. Phys. Exp.*, vol. 6, no. 6, 2013, Art. no. 062102.
[15] Y. Zhao *et al.*, "Indium incorporation and emission properties of nonpolar and semipolar ingan quantum wells," *Appl. Phys. Lett.*, vol. 100, no. 20, 2012, Art. no. 201108.
[16] H. Fu, Z. Lu, and Y. Zhao, "Analysis of low efficiency droop of semipolar InGaN quantum well light-emitting diodes by modified rate equation with weak phase-space filling effect," *AIP Adv.*, vol. 6, no. 6, 2016, Art. no. 065013.
[17] J. Vuckovic, M. Loncar, and A. Scherer, "Surface plasmon enhanced light-emitting diode," *IEEE J. Quantum Electron.*, vol. 36, no. 10, pp. 1131–1144, Oct. 2000.
[18] K. Okamoto, I. Niki, A. Shvartser, Y. Narukawa, T. Mukai, and A. Scherer, "Surface-plasmon-enhanced light emitters based on InGaN quantum wells," *Nature Mater.*, vol. 3, no. 9, pp. 601–605, 2004.
[19] X. Feng, F. Liu, and Y. Huang, "Calculated plasmonic enhancement of spontaneous emission from silicon nanocrystals with metallic gratings," *Opt. Commun.*, vol. 283, no. 13, pp. 2758–2761, 2010.
[20] M. Nami and D. Feezell, "Optical properties of Ag-coated GaN/InGaN axial and core–shell nanowire light-emitting diodes," *J. Opt.*, vol. 17, no. 2, 2015, Art. no. 025004.
[21] M. Nami and D. F. Feezell, "Optical properties of plasmonic light-emitting diodes based on flip-chip III-nitride core-shell nanowires," *Opt. Exp.*, vol. 22, no. 24, pp. 29445–29455, 2014.
[22] X. Wang *et al.*, "Continuous-flow MOVPE of Ga-Polar GaN column arrays and core–shell led structures," *Cryst. Growth Des.*, vol. 13, no. 8, pp. 3475–3480, 2013.
[23] A.-L. Bavencove *et al.*, "Light emitting diodes based on GaN core/shell wires grown by MOVPE on n-type Si substrate," *Electron. Lett.*, vol. 47, no. 13, pp. 765–767, 2011.
[24] A. Maslov and C.-Z. Ning, "Size reduction of a semiconductor nanowire laser by using metal coating," *Proc. SPIE*, vol. 6468, 2007, Art. no. 64680I.
[25] S. A. Maier, "Plasmonic field enhancement and SERS in the effective mode volume picture," *Opt. Exp.*, vol. 14, no. 5, pp. 1957–1964, 2006.
[26] R. F. Oulton, V. J. Sorger, D. Genov, D. Pile, and X. Zhang, "A hybrid plasmonic waveguide for subwavelength confinement and long-range propagation," *Nature Photon.*, vol. 2, no. 8, pp. 496–500, 2008.
[27] R. Ruppin, "Electromagnetic energy density in a dispersive and absorptive material," *Phys. Lett. A*, vol. 299, no. 2, pp. 309–312, 2002.
[28] M. G. Blaber, M. D. Arnold, and M. J. Ford, "Search for the ideal plasmonic nanoshell: The effects of surface scattering and alternatives to gold and silver," *J. Phys. Chem. C*, vol. 113, no. 8, pp. 3041–3045, 2009.

[29] K. Ding and C.-Z. Ning, "Metallic subwavelength-cavity semiconductor nanolasers," *Light: Sci. Appl.*, vol. 1, no. 7, 2012, Art. no. e20.
[30] K. Ding *et al.*, "Room-temperature continuous wave lasing in deep-subwavelength metallic cavities under electrical injection," *Phys. Rev. B*, vol. 85, no. 4, 2012, Art. no. 041301.
[31] C.-Y. Lu and S. L. Chuang, "A surface-emitting 3D metal-nanocavity laser: Proposal and theory," *Opt. Exp.*, vol. 19, no. 14, pp. 13225–13244, 2011.
[32] A. Waag *et al.*, "The nanorod approach: GaN nanoLEDs for solid state lighting," *Phys. Status Solidi c*, vol. 8, no. 7/8, pp. 2296–2301, 2011.
[33] S. Shokhovets *et al.*, "Determination of the anisotropic dielectric function for wurtzite AlN and GaN by spectroscopic ellipsometry," *J. Appl. Phys.*, vol. 94, no. 1, pp. 307–312, 2003.
[34] M. T. Hill *et al.*, "Lasing in metal-insulator-metal sub-wavelength plasmonic waveguides," *Opt. Exp.*, vol. 17, no. 13, pp. 11107–11112, 2009.
[35] A. Maslov and C.-Z. Ning, "Reflection of guided modes in a semiconductor nanowire laser," *Appl. Phys. Lett.*, vol. 83, no. 6, pp. 1237–1239, 2003.
[36] K. Ding *et al.*, "Room-temperature continuous wave lasing in deep-subwavelength metallic cavities under electrical injection," *Phys. Rev. B*, vol. 85, no. 4, 2012, Art. no. 041301.